Duplex Printing of All-in-One Integrated Electronic Device for Temperature Monitoring

Jingxin Zhao[a,b,c], Yan Zhang[a], Yinan Huang[c] Xiaoxin Zhao[a], Yunhui Shi[a], Jingyi Qu[a], Chengfeng Yang[a], Jixun Xie[a], Juanjuan Wang[a], Lele Li[a], Qinghai Yan[a], Shihui Hou[a], Conghua Lu*[a], Xinhua Xu*[a], Yagang Yao*[b,c]

a. School of Materials Science and Engineering, Tianjin University, Tianjin, 300072, P. R. China

b. National Laboratory of Solid State Microstructures, College of Engineering and Applied Sciences, and Collaborative Innovation Center of Advanced Microstructures, Nanjing University, Nanjing 210093, China

c. Division of Advanced Nanomaterials, Joint Key Laboratory of Functional Nanomaterials and Devices, Key Laboratory of Nanodevices and Applications, CAS Center for Excellence in Nanoscience, Suzhou Institute of Nano-tech and Nano-bionics, Chinese Academy of Sciences, Suzhou 215123, P. R. China

d. Suzhou Institute of Nano-Tech and Nano-Bionics Nanchang, Chinese Academy of Sciences, Nanchang 330200, P. R. China

E-mail: [*] ygyao2013@sinano.ac.cn

chlu@tju.edu.cn

xhxutju@gmail.com

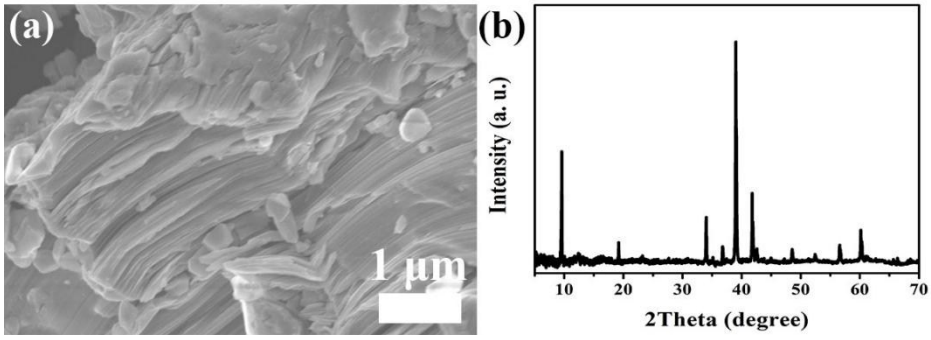

Fig. S1 The structure characterization of the pristine Ti_3AlC_2 phase.

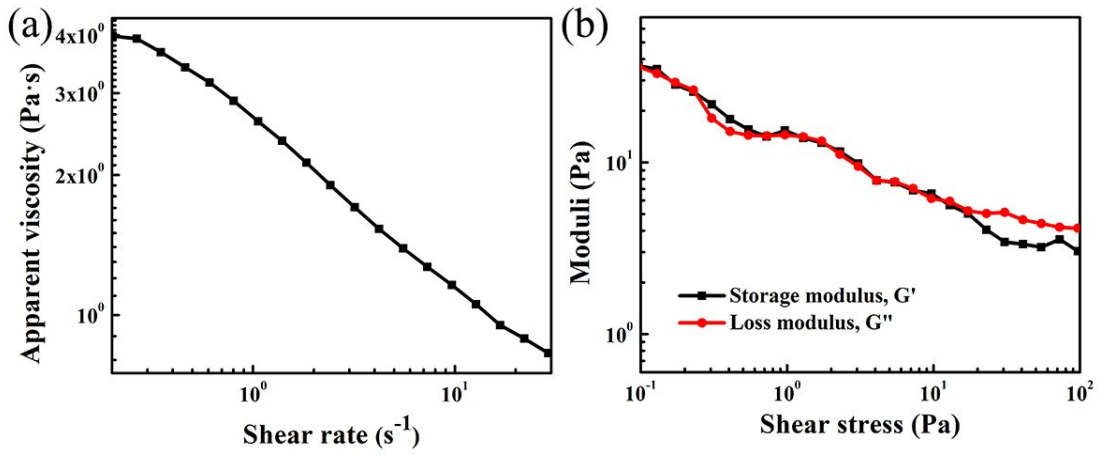

Fig. S2 (a) and (b) Apparent viscosity as a function of shear rate for rGO/SWCNTs ink and storage modulus, G', and loss modulus, G'', as a function of shear stress for rGO/SWCNTs ink after 4 weeks of storage.

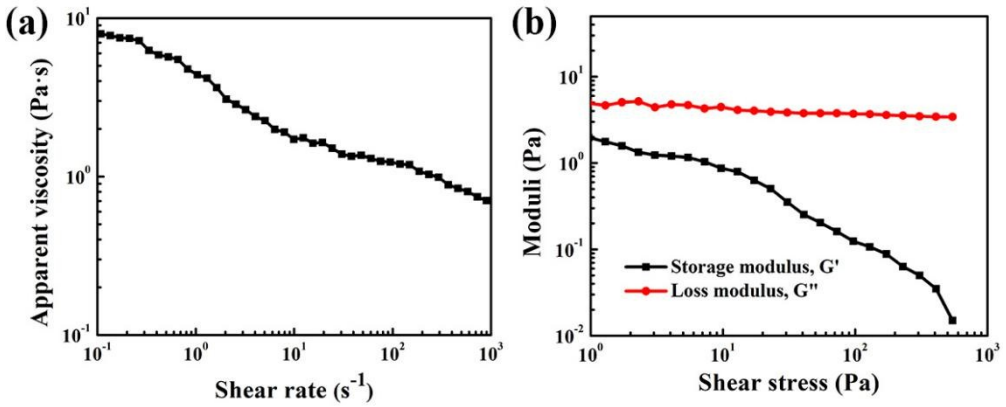

Fig. S3 Rheological properties of electrolyte ink. (a) Apparent viscosity as a function of shear rate. (b) Storage modulus, G′, and loss modulus, G″, as a function of shear stress.

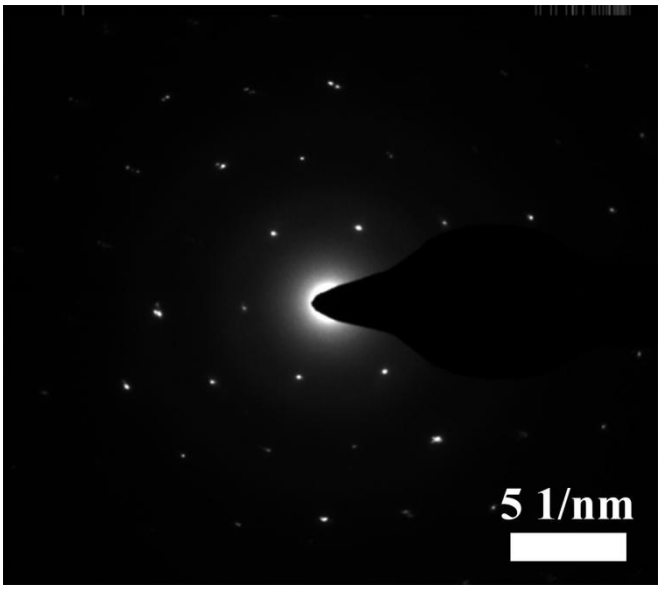

Fig. S4 Corresponding selected area electron diffraction of the as-prepared MXenes.

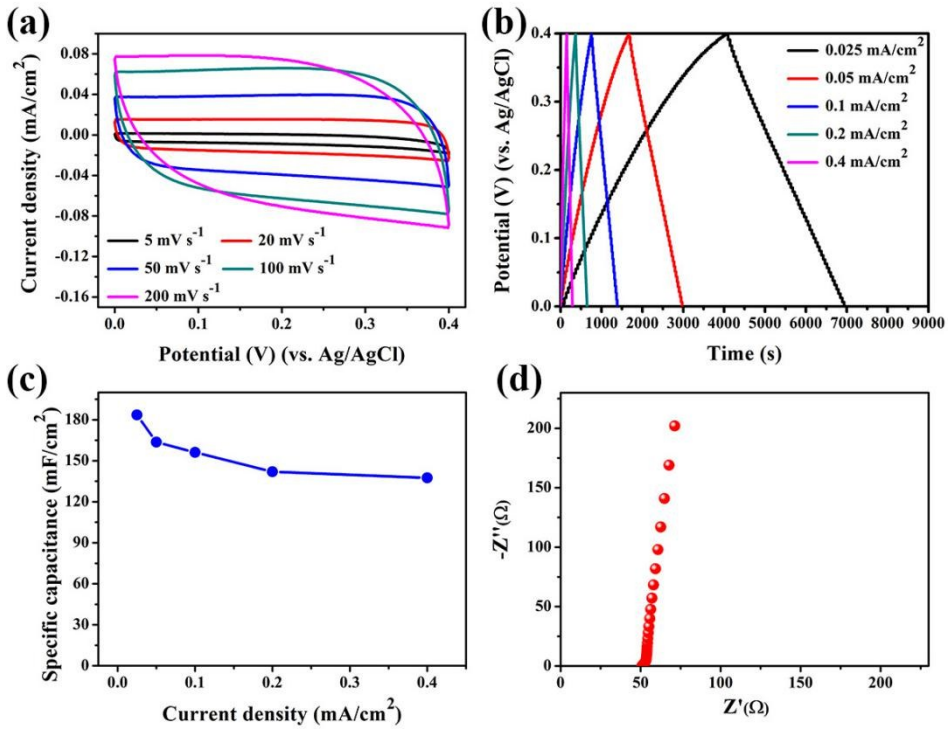

Fig. S5 (a) CV curves of MXenes/SWCNTs at different scan rate. (b) GCD curves at different current densities. (c) rate capability. (d) Nyquist plot.

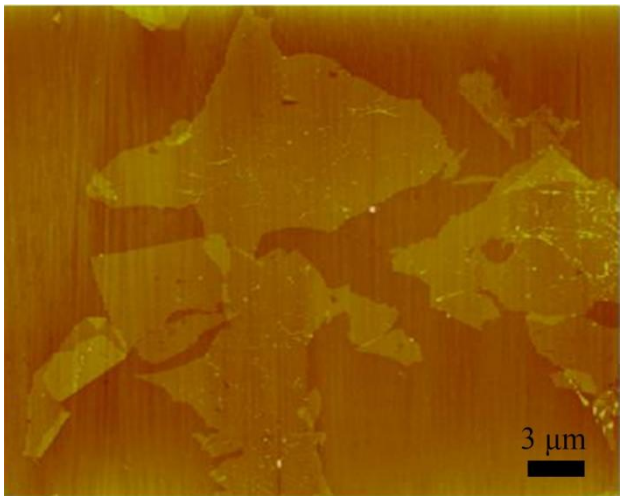

Fig. S6 Typical atomic force microscopy image of rGO sheets.

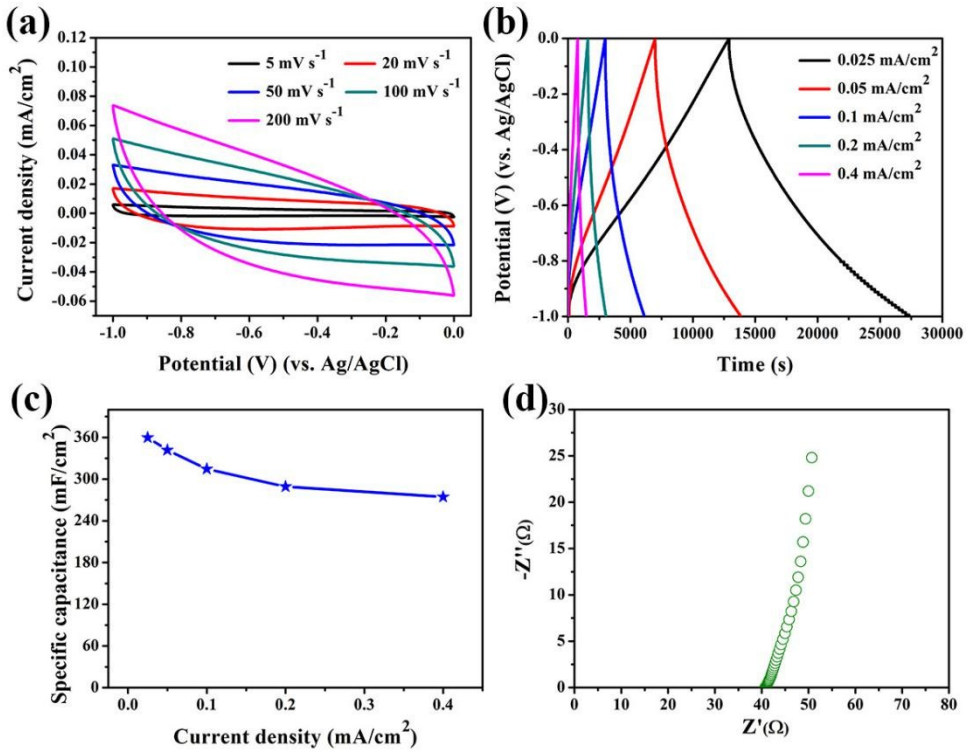

Fig. S7 (a) CV curves of rGO/SWCNTs at different scan rate. (b) GCD curves at different current densities. (c) rate capability. (d) Nyquist plot.

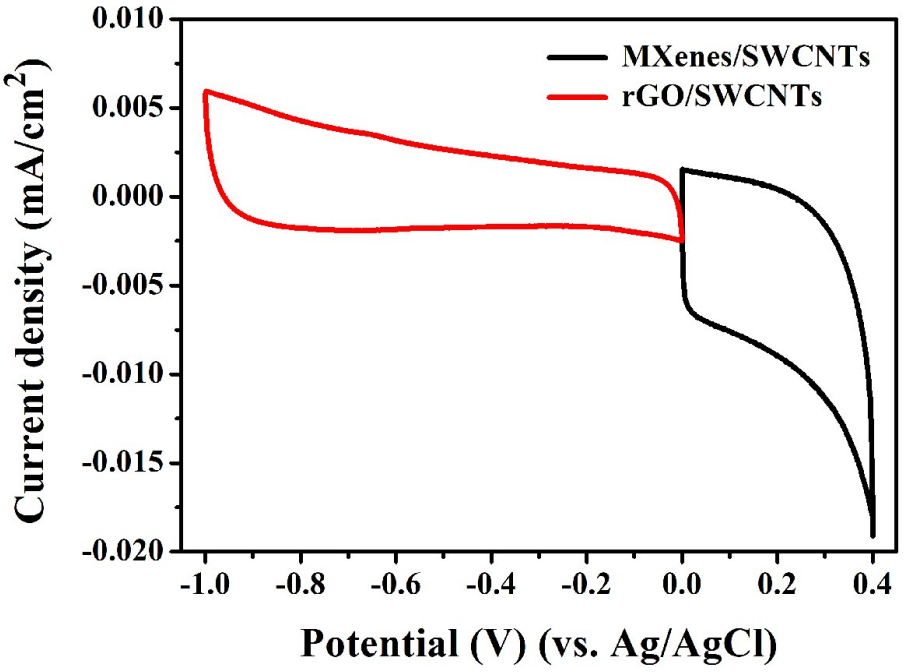

Fig. S8 Comparative CV curves obtained for the MXenes/SWCNTs and rGO/SWCNTs at a scan rate of 5 mVs^{-1} in a three-electrode system.

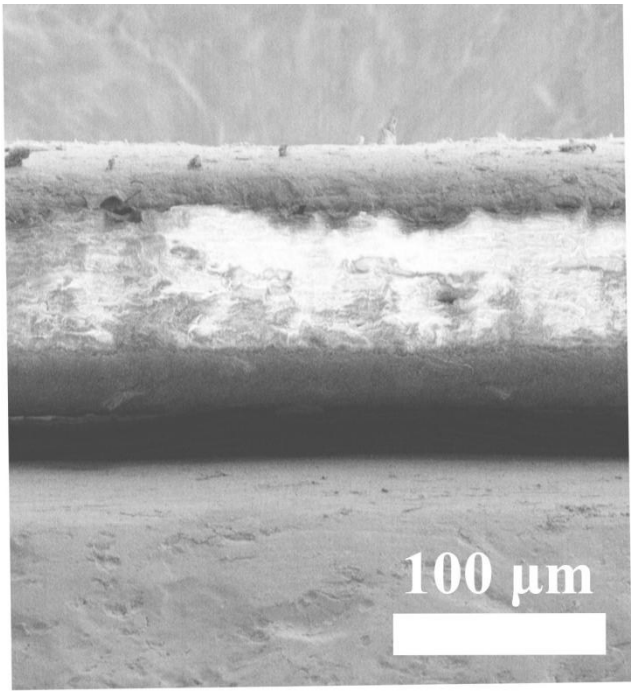

Fig. S9 SEM cross-sectional image of the MXenes/SWCNTs electrode.

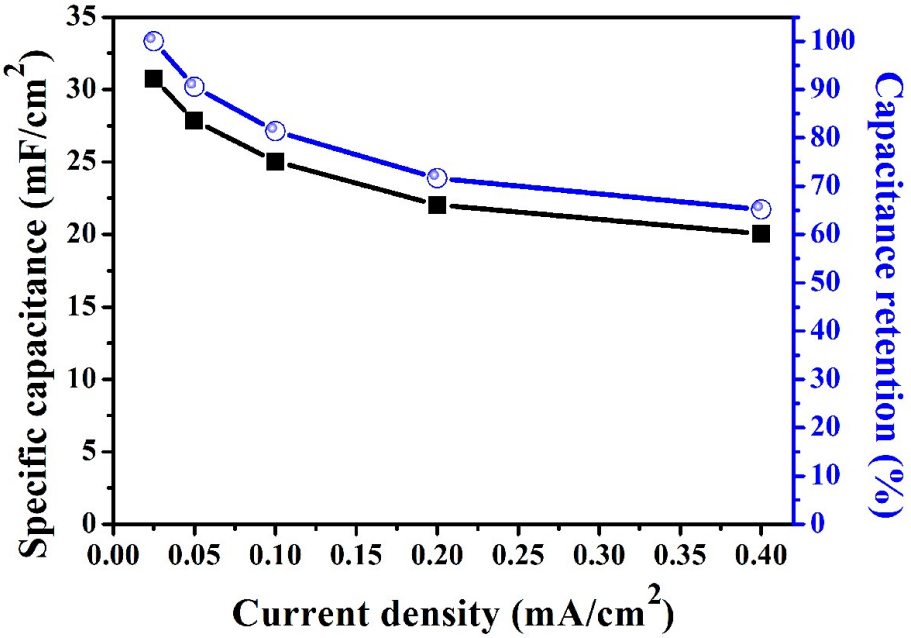

Fig. S10 Areal specific capacitance and capacitive retention of the assembled device calculated as a function of current density.

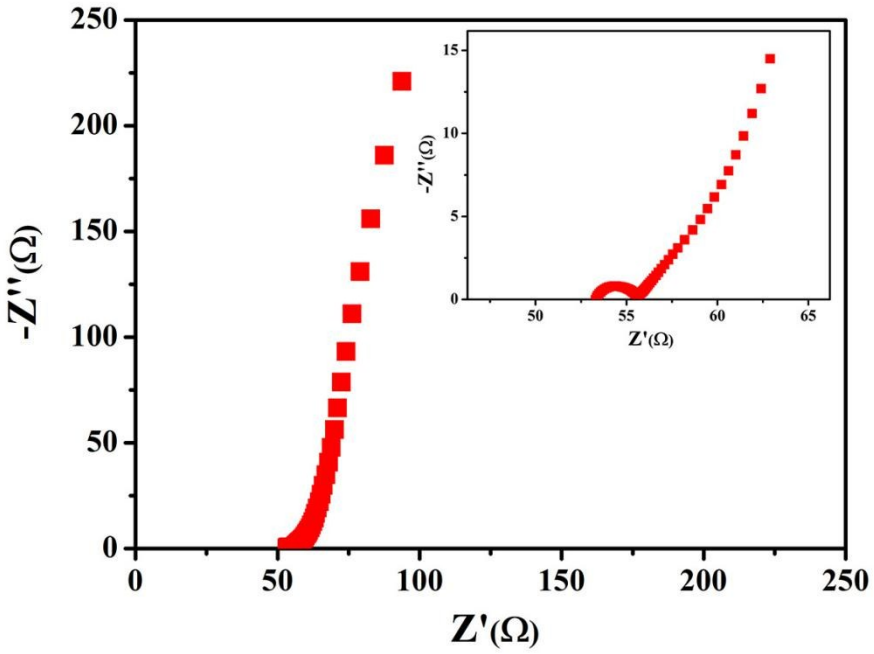

Fig. S11 Nyquist plot of 3D printing asymmetric MSCs.

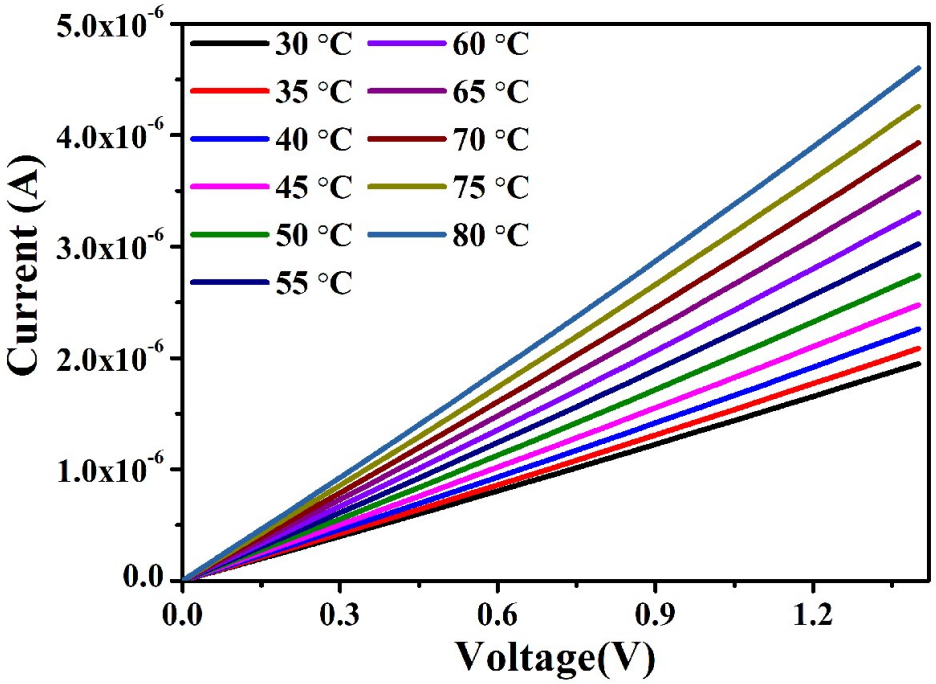

Fig. S12 *I-V* curves of the integrated device between 30 ℃ to 80 ℃ (temperature steps set as 5 ℃ for clarity).

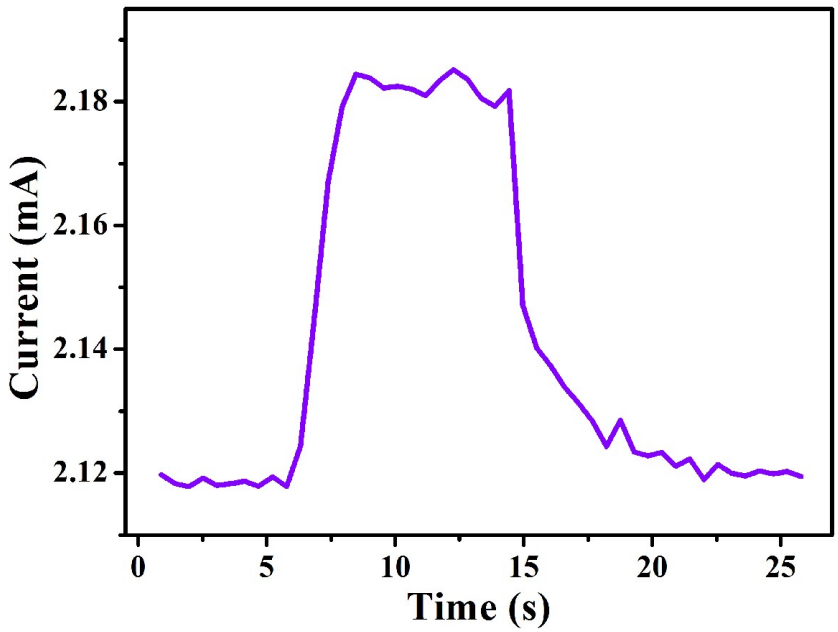

Fig. S13 Rapid response/recovery time of integrated configuration.

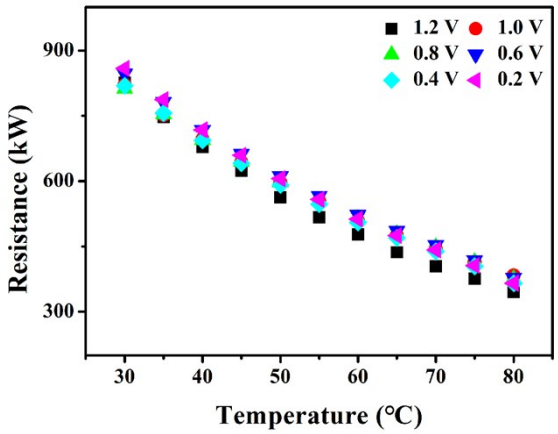

Fig. S14 The curves of resistance varitaion with temperature on different voltage.

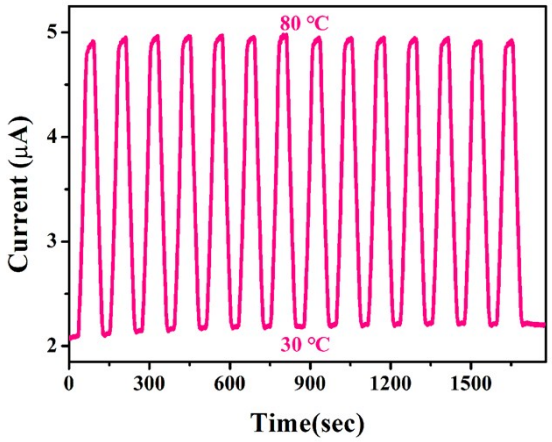

Fig. S15 The repeatability of the integrated configuration.

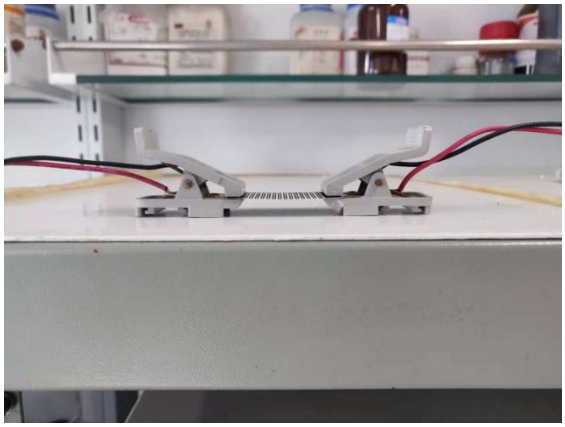

Fig. S16 The operation picture of integrated device.

The CV curves of rGO/SWCNTs negative electrode taken between -1.0 and 0 V in 1 M H_3PO_4 electrolyte at different scan rates are shown in Fig. S6a, which indicates excellent capacitive performance of the rGO/SWCNTs negative electrode. The results of GCD measurement exhibits the nearly symmetric triangular shapes at different current densities of 0.025-0.4 mA cm^{-2}, demonstrating the ideal capacitive behavior (Figure S6b). Meantime, an initial capacitance retention of 76.2% can be still retained even at a high current density of 0.4 mA cm^{-2} (Figure S6c). Moreover, the rGO/SWCNTs possesses a smaller intrinsic resistance (R_b) value of approximately 40.69 Ω (Figure S6d).